Trade-off on Fuel Economy, Knock, and Combustion Stability for a Stratified Flame-ignited Gasoline Engine

Kang Song, Xinyan Wang, and Hui Xie*

Abstract

A combination of port fuel injection (PFI) and direct injection (DI), called P-DI strategy, was used in a four-cylinder gasoline engine. The aim was to achieve a stratified flame ignition (SFI) hybrid combustion and manage the trade-off among fuel economy, knock, and combustion stability (EKS) in a gasoline engine. In the proposed P-DI strategy, DI was used to enrich the local mixture around the spark plug to enhance the early spark-ignition combustion. On the other hand, PFI was used to form a largely lean homogeneous mixture to achieve a moderately controlled auto-ignition combustion in the outer region of the cylinder. The effects of DI fraction (R_{DI}) and start of injection (SOI) timing of DI on the SFI hybrid combustion were investigated experimentally. It was found that an increased R_{DI} resulted in a parabolic-like effect on the combustion phasing and combustion stability. The earliest combustion phasing was achieved with an R_{DI} of approximately 35%. The fuel economy deteriorated monotonously with increasing R_{DI}. In comparison, the effect of SOI on the SFI hybrid combustion was more complicated. It was found that an SOI between 50 °CA before top-dead-center (BTDC) and 90 °CA BTDC showed a potential to achieve a satisfactory trade-off among EKS. Based on the above findings, a cost function (J) was proposed to represent the EKS trade-off and reduce the calibration burden for optimal SOI at different engine operating conditions. An extremum-seeking algorithm was adopted to search for the maximum value of J and obtain the optimal SOI timing at each operating point. The proposed algorithm was then validated by experimental results.

Key words: Hybrid combustion, Stratified mixture, Controlled auto-ignition, Port direct injection, Injection timing optimization.

1 Introduction

A controlled auto-ignition (CAI) combustion process [1] has the potential to simultaneously reduce both fuel consumption and nitrogen oxide emissions. However, this process is very sensitive to operating conditions [2], which limit the operating range [3-5] of this combustion mode. The spark-ignition (SI)–CAI hybrid combustion [6-8] is a promising solution, because it can initiate combustion with a slow flame propagation followed by a rapid multi-site auto-ignition. By employing the SI–CAI hybrid combustion, the upper load limit can be extended [7, 9] and a smooth transition between SI combustion and CAI combustion can be achieved [7, 9-11]. The effects of spark timing (ST) [12, 13], intake temperature [14], and dilution charge [15] on the hybrid combustion process were also widely investigated. Despite the aforementioned benefits, the upper load limit of the SI–CAI hybrid combustion is still limited due to the unacceptable maximum pressure rise rate (PRR_{max}) at some loading conditions with homogenous in-cylinder mixture [9]. Retarding the combustion phasing can reduce PRR_{max}; however, it can increase cyclic combustion variations [9, 15, 16] as a retarded combustion is not robust enough to accommodate cycle-to-cycle variations of in-cylinder conditions [17]. In addition, an over-retarded combustion phasing would also lead to fuel penalty.

In order to address the aforementioned trade-off among fuel economy, PRR_{max} (which is a simplified indication of knock intensity), and combustion stability, denoted as economy-knock-stability (EKS) trade-off, previous investigations were performed from two aspects: 1) to understand the causes of combustion instability and 2) to seek an effective solution for the EKS trade-off.

Reuss et al. [18] found that an early kernel growth (EKG) period played a dominant role in the combustion phasing variation for SI-CAI hybrid combustion based on the results at 2000 rpm and 2 bar indicated mean effective pressure (IMEP) on an optical engine. Using the same data from Reuss et al. [18], Natarajan et al. [19] suggested that the fuel/air distribution and its velocity at the vicinity of the spark plug were crucial for a stable combustion in the EKG period. By using three-dimensional computational fluid dynamics simulations, Wang et al. [20] demonstrated that the flame propagation and subsequent auto-ignition were sensitive to the in-cylinder turbulent kinetic energy level and the mean flow velocity around the spark plug at 1500 rpm and 3.6 bar IMEP. Experimental results from Chen et al. [21] indicated that the maximum cyclic combustion variation occurs in the initial heat release phase, as measured by the crank angle of 10% accumulated heat release (CA10) at 1500 rpm and 6 bar IMEP. Hellstrom et al. [22] and Yoshizawa et al. [17] suggested that the cyclic coupling of in-cylinder states, such as the thermal energy and unburned fuel, is the main cause [22] of combustion variation. Those findings indicated the potential for stabilizing the SI-CAI hybrid combustion by enhancing the initial flame propagation process.

Fuel stratification is one of the most effective solutions [3, 23] to address the EKS trade-off by increasing the combustion duration with a lower knock intensity. Yun et al. [16] applied a dual-pulse direct injection (DI) to achieve fuel stratification with a largely stoichiometric air–fuel mixture and found that the trade-off between combustion noise (related to knock intensity) and combustion stability can be slightly improved. However, the authors found that retarding the second DI with a fixed fuel rate could deteriorate the fuel economy. In addition, they also found that soot and carbon monoxide emissions were monotonically increased as the second injection timing was retarded [16]. Similarly, the dual-pulse DI was also adopted by Yoshizawa et al. [17] to achieve the so-called two-phase combustion with a largely lean air–fuel mixture, which was shown to be effective in preventing knocks. Despite the benefit of the dual-pulse DI, pure DI showed a higher particulate number emission compared to port fuel injection (PFI), as indicated in the experimental study reported in [24].

In addition to the DI strategy, a combined PFI and DI (P-DI) strategy was applied in a gasoline engine to enable a stratified flame ignition (SFI) hybrid combustion [25, 26]. In the proposed SFI hybrid combustion concept, DI was used to form a rich mixture around the spark plug in the central region of the combustion chamber and stabilize the flame kernel formation and initial flame propagation. On the other hand, PFI was used to provide a lean homogenous mixture in the peripheral region and achieve a relatively moderate CAI combustion process [25, 26]. The moderate heat release rate (HRR) of the SFI hybrid combustion would reduce the risk of knocking and offers a potential to improve the fuel economy by advancing the combustion phasing. In addition, as a part of the fuel is provided by PFI in the P-DI strategy, the soot emission could be reduced due to a more homogeneous fuel–air mixture in the cylinder compared to that of the pure DI strategy [24, 27]. Meanwhile, the fraction of fuel mass from DI (R_{DI}) in the total fuel mass and the corresponding start of injection (SOI) timing of DI in the P-DI strategy can be varied to control the SFI combustion process [28].

As discussed in the above literature review, although the SFI combustion concept has been proposed to stabilize the SI-CAI combustion in gasoline engines [25, 26], there is still a lack of experimental investigation on the benefits of the P-DI strategy over the pure PFI and pure DI strategies. Most importantly, there is a gap between the concept of SFI hybrid combustion and its practical application to the engine where an advanced control algorithm is required in order to tackle the complex control problems in SFI hybrid combustion. Therefore, the SFI hybrid combustion achieved using the P-DI strategy is compared with the SI-CAI hybrid combustion achieved using the pure PFI and DI strategies in a four-cylinder gasoline engine. Then, the effects of the DI fraction and the SOI timing of DI on the EKS trade-off of SFI hybrid combustion by using the P-DI strategy are investigated in detail. To realize the SFI hybrid combustion in a real engine application, a cost function is proposed to mathematically describe the EKS trade-off of the SFI hybrid combustion and address the complexity in the calibration of the

optimal SOI timing. Using the proposed cost function, an online optimization algorithm is developed based on an extremum seeking (ES) algorithm [29], which is used to seek the corresponding optimal SOI timing in real time. Finally, the effectiveness of the proposed control method is experimentally validated.

2 Engine test bench setup

The operating principle of SFI hybrid combustion is briefly illustrated in Fig. 1. The negative valve overlap (NVO) strategy was used to trap the hot internal exhaust gas recirculation (EGR) to trigger the CAI combustion. The spark plug was used to initiate the early-stage SI combustion. In order to attain fuel stratification, the P-DI system was applied in conjunction with a shallow bowl piston.

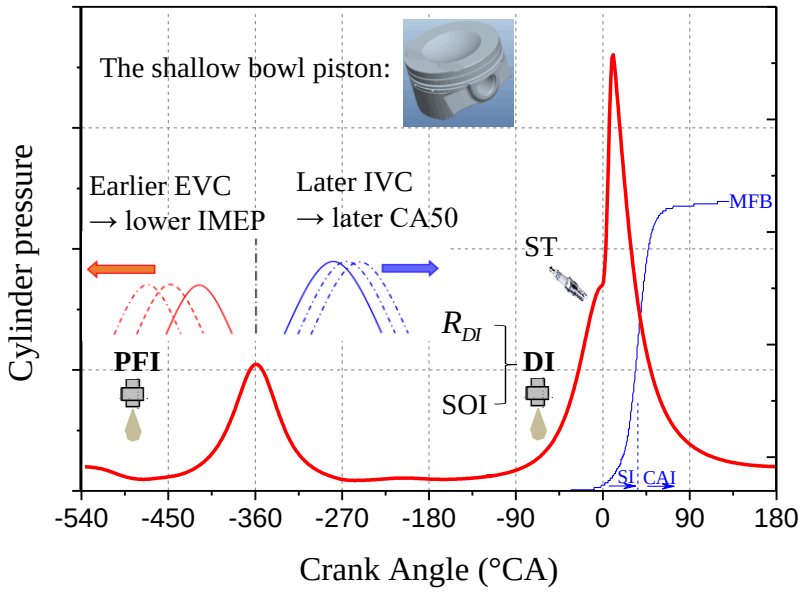

Fig. 1 Operating principle of P-DI-enabled SFI hybrid combustion. IVC: intake valve closing; CA50: crank angle at 50% cumulative heat release; ST: spark timing; MFB: mass fraction burnt.

SFI hybrid combustion was performed in a 2.0 L turbocharged four-cylinder engine equipped with the P-DI system. The engine specifications are listed in Table 1, and the test cell schematic is shown in Fig. 2. The other test devices are listed in Table 2. The SI-CAI hybrid combustion and different fuel injection strategies were applied in four cylinders, but only one cylinder was measured in the experiments. Here, 0 °CA ATDC refers to the top dead center at the end of the compression stroke.

Table 1. Engine specifications.

Geometry compression ratio	9.6:1
Cylinder bore	82.5 mm

Stroke	92 mm
Intake valve opening duration	160 °CA
Intake valve lift	6 mm
Exhaust valve opening duration	120 °CA
Exhaust valve lift	4 mm
PFI injection timing	500 °CA BTDC
SOI timing of DI	0–240 °CA BTDC
Piston	With shallow bowl (Fig. 1)
Fuel	Commercial gasoline 95 RON
DI Injector	Delphi Multec®, six-hole, side mounted
Coolant temperature	95±2°C
Ambient temperature	25±2°C

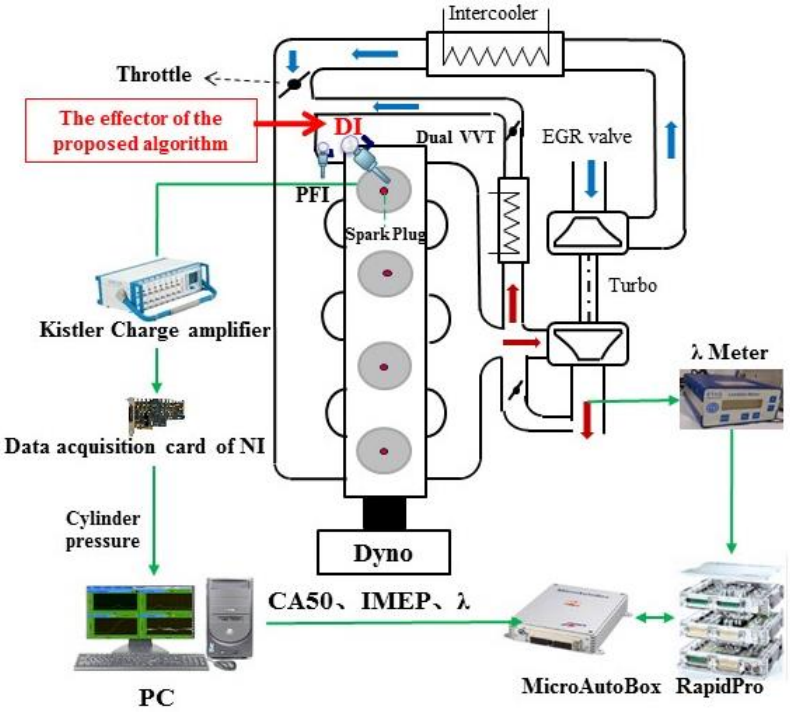

Fig. 2 The gasoline engine platform.

Table 2. Test equipment and methods.

Cylinder pressure measurement	Kistler 6053c pressure sensor sampled by the National Instrument data acquisition card (PCI6123) triggered by 3600 pulse/revolution optical encoder
Combustion analysis system	In-house developed Labview code
Control system	MicroAutoBox of dSPACE
Excessive air ratio measurement	Linear oxygen sensor (LSU4.9, ETAS)
External EGR (eEGR) rate	Calculated based on carbon dioxide concentration in the intake and exhaust manifold by the combustion NDIR500 sensor

3 Study of the SFI hybrid combustion process

3.1 Comparison of EKS trade-off for PFI, DI, and P-DI strategies

The SFI hybrid combustion process with the P-DI strategy was analyzed in detail and compared with the SI-CAI hybrid combustion with pure PFI and DI strategies. The operating conditions are given in Table 3, and the results are shown in Fig. 3. The combustion phasing, defined as the crank angle at 50% cumulative heat release (CA50), was swept by adjusting the ST and intake valve closing (IVC) timing, as indicated in Table 3. In addition, the SOI timing was also varied for the P-DI strategy. Lambda was fixed as 1 for all the experiments by controlling the intake air mass flow rate through the adjustment of the throttle position. The operating window of CA50 and IMEP with PRR_{max} < 5 bar/°CA and coefficient of variation COV(IMEP) < 5% are shown in Fig. 3 and the quantitative results are listed in Table 4 for the different strategies.

Table 3. Operating conditions for PFI, P-DI, and DI strategies at 1500 rpm.

	PFI	P-DI	DI
Fuel rate (mg/stroke)	18.95	18.95	18.95
Lambda	1	1	1
Spark Timing (°CA BTDC)	[2, 10]	[4, 11]	[6, 14]
IVC timing (°CA ATDC)	[603, 613]	589	[583, 589]
EVC timing (°CA ATDC)	310	310	310
SOI of DI (°CA BTDC)	-	[60, 120]	280
Rail pressure (bar)	-	80	80
eEGR rate (%)	0	0	0

Table 4. Operating range for PFI, P-DI, and DI strategies.

	PFI	DI	P-DI
CA50 window (°CA ATDC)	[19.8, 24.6]	[17.8, 24]	[17.2, 21.9]
Average CA50 in CA50 window (°CA ATDC)	22.2	20.9	19.55
IMEP window (bar)	[5.11, 5.34]	[4.97, 5.26]	[5.16, 5.33]
Average IMEP in CA50 window (bar)	5.22	5.12	5.25
IMEP at CA50 = 20 °CA ATDC (bar)	5.33	5.16	5.25
PRR_{max} at CA50 = 20 °CA ATDC (bar/°CA)	4.89	3.6	3.5
COV(IMEP) at CA50 = 20 °CA ATDC (%)	3.48	3.63	4.35

Overall, for each fuel injection strategy, advancing the CA50 led to a higher IMEP at the expense of increased PRR_{max}. Compared to the P-DI and DI strategies, the PFI strategy showed a later CA50 in order to control PRR_{max} below 5 bar/°CA. This could be attributed to the rapid multi-site auto-ignition of the homogenous mixture with the PFI strategy. For the pure DI strategy, the CA50 window was earlier than that of the PFI strategy as shown in Fig. 3. The earlier CA50 with DI strategy could be the result of certain fuel stratification in the cylinder by using early DI during intake stroke [30, 31]. In addition, the early DI during intake stroke also affected the IMEP range ([4.97, 5.26] compared to [5.11 to 5.34] with PFI) with a relative deterioration of 1.5% to 2.5%. This was considered as the result of wall wetting due to DI.

Compared to the PFI and DI strategies, the P-DI strategy combined the advantages of both PFI and DI strategies with the earliest CA50 window and highest IMEP. As indicated in Table 3, with a fixed fuel rate, the average CA50 in the available CA50 window with P-DI strategy was 2.65 °CA earlier than that with the PFI strategy and 1.35 °CA earlier than that with the DI strategy. The average IMEP in the available CA50 window with the P-DI strategy was 0.4% higher than that with the PFI strategy and 2.5% higher than that with the DI strategy. Therefore, the P-DI strategy achieved higher IMEP values with acceptable COV(IMEP) and PRR_{max}. With CA50 = 20 °CA ATDC, the P-DI strategy achieved a much lower PRR_{max} compared to that with PFI, while producing a higher IMEP than that with DI.

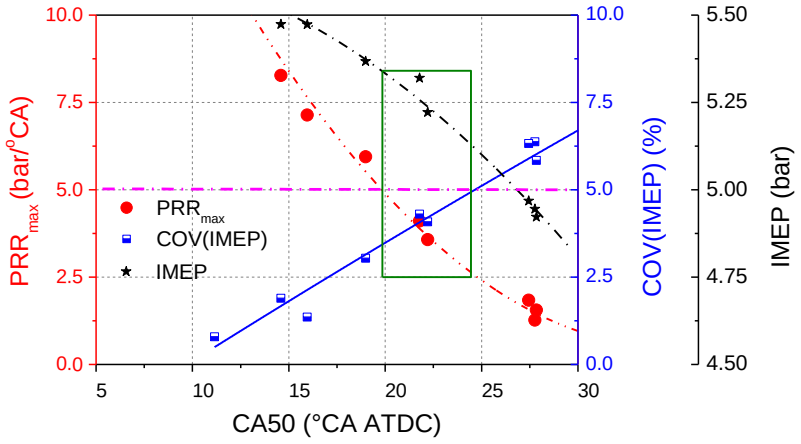

(a) PFI strategy

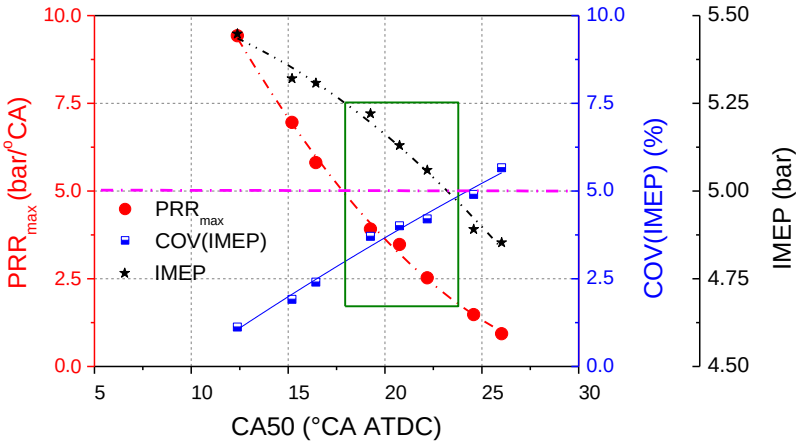

(b) DI strategy

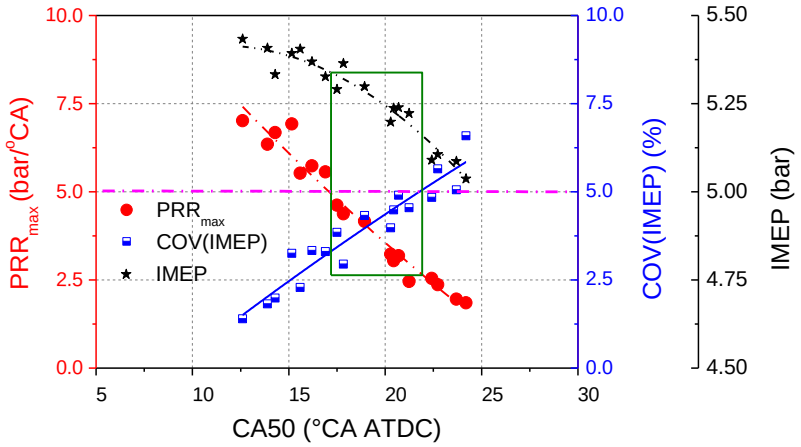

(c) P-DI strategy

Fig. 3 Comparison of EKS trade-off for (a) PFI, (b) DI, and (c) P-DI strategies.

To understand the aforementioned benefits of the P-DI strategy, two engine test points with the same CA50 were selected from P-DI and PFI strategies and compared in detail. The main operating conditions of the two selected operating points are given in Table 5.

Table 5. Operating conditions for selected operating points with P-DI and PFI strategies.

	PFI	P-DI
R_{DI} (%)	0	25
SOI of DI (°CA BTDC)	-	60
IVC (°CA ATDC)	589	589
ST (°CA ATDC)	6	8

Fig. 4 shows a comparison of the HRR profiles and in-cylinder pressure traces of the selected two operating points with PFI and P-DI strategies. It can be observed that the P-DI strategy produced a slightly faster HRR at the early stage from −5 to 12 °CA ATDC, which also led to the higher in-cylinder pressure. This result indicated that the P-DI strategy could be used to enhance the early flame kernel formation and the flame propagation process. After 12 °CA ATDC, the HRR with the P-DI strategy gradually reduces, and the peak HRR becomes lower than that with the PFI strategy. As a result, the P-DI strategy produced a more moderate in-cylinder pressure trace with a lower PRR and peak in-cylinder pressure than the PFI strategy. The observed reduction in the subsequent heat release process could be attributed to the lean mixture at the outer region of the cylinder due to the fuel stratification by the P-DI strategy. In terms of combustion stability, compared to the PFI strategy, the P-DI strategy shows a little effect on the COV(IMEP) and the standard deviation of CA50 for the test points shown in Fig. 4.

Therefore, the proposed P-DI-enabled SFI combustion could achieve a lower PRR_{max} at the same CA50 than the conventional PFI-enabled SI-CAI hybrid combustion. Thus, it could be used to extend the upper load limit and allow an earlier CA50 to improve the fuel economy. To some extent, the P-DI-enabled SFI combustion offers an additional control method to address the EKS trade-off by introducing a controllable fuel stratification.

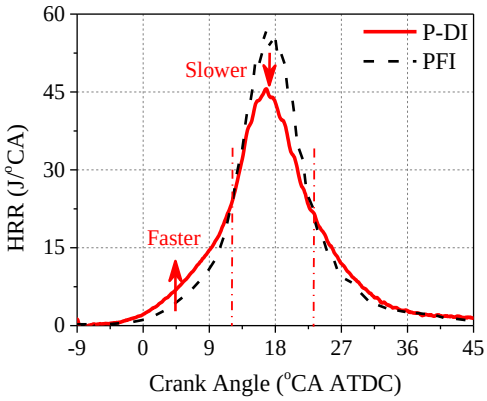

(a) Heat release rate

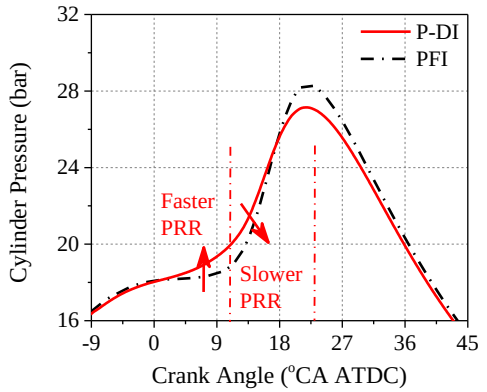

(b) In-cylinder pressure

Fig. 4 Comparison of (a) heat release rate (HRR) and (b) in-cylinder pressure with PFI and P-DI strategies at CA50 (18.9 °CA ATDC).

3.2 Effect of control parameters on SFI hybrid combustion with P-DI strategy

The effects of the DI fraction (R_{DI}) and SOI timing of DI on the EKS trade-off were investigated for the SFI hybrid combustion. The findings will be used for the controller design of the closed-loop control, which will be discussed in the next section. It should be noted that the upper limit of PRR_{max} was set as 5 bar/°CA and a combustion with PRR_{max} exceeding this limit was regarded as knocking combustion. The upper limit of COV(IMEP) was set as 5% and the operating points with COV(IMEP) over this limit was regarded as unstable combustion.

3.2.1 Effect of DI fraction (R_{DI})

To understand the effect of DI fraction on the EKS trade-off, a sweep of the DI fraction from 0% to 39% was performed. The operating conditions are presented in Table 6. It should be noted that DI fractions less than 23% were not achievable due to the limitation of the fuel flow rate control capability with the adopted solenoid injector. DI fractions greater than 39% were

not included as the fuel economy became worse. The HRR profiles are shown in Fig. 5 and the corresponding IMEP, COV(IMEP), CA50, and PRR_{max} are shown in Fig. 6.

Table 6. Operating conditions for the study on the effect of DI fraction (R_{DI}).

Engine speed (rpm)	1500
Fuel rate (mg/stroke)	18.95
SOI of DI (°CA BTDC)	50
DI fraction (%)	0, 23, 30, 35, and 39
IVC (°CA ATDC)	589
EVC (°CA ATDC)	[310, 313]
eEGR rate (%)	0
Intake manifold pressure (bar)	1.06–1.07
Spark timing (°CA BTDC)	6
Overall lambda (-)	1
Common rail pressure (bar)	80

As shown in Fig. 5, the increase in DI fraction from 0% (PFI only) to 35% led to an earlier combustion phasing. The main reason could be the richer fuel–air mixture around the spark plug at a higher DI fraction, which could enhance the early heat release from the flame propagation [25, 26]. Compared with the DI fraction of 30%, the DI fraction of 35% produced a more moderate heat release process with a lower peak HRR value although its CA50 was even slightly earlier. This could be caused by the leaner mixture in the peripheral area due to the larger DI fraction. As the DI fraction increased to 39%, the corresponding combustion process was significantly retarded and became even weaker than the baseline PFI case, as shown in Fig. 5. This could be attributed to the DI cooling effect and the over-rich mixture around the spark plug; however, the over-lean mixture around the cylinder inhibited the entire hybrid combustion process [25].

Fig. 6 shows a comparison of the CA50, IMEP, COV(IMEP), and PRR_{max} at different DI fractions. It was found that the increase in DI fraction from 0 to 35% led to a gradually advanced CA50 while a further increase to 39% led to a significantly delayed CA50. In comparison, IMEP and PRR_{max} decreased with the DI fraction, which could be attributed to the incomplete combustion due to the increased amount of late DI. PRR_{max} could be controlled below 5 bar/°CA for all the tested DI fractions. Therefore, the smallest DI fraction could be applied to ensure a better thermal efficiency of the SFI hybrid combustion.

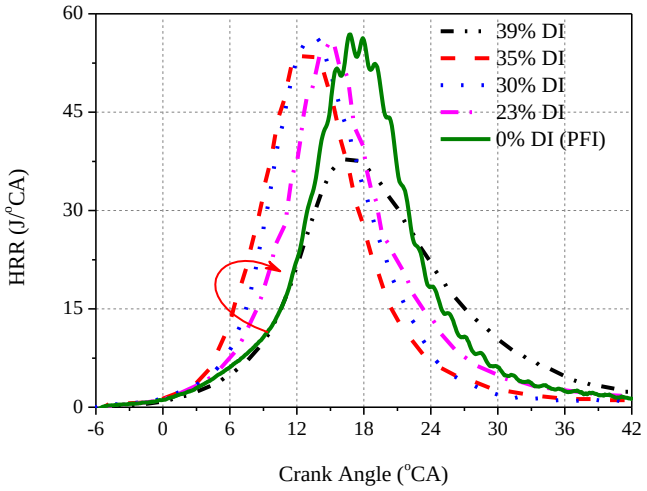

Fig. 5 Effect of DI fraction on HRR with SOI = 50 °CA BTDC and ST = 6 °CA BTDC.

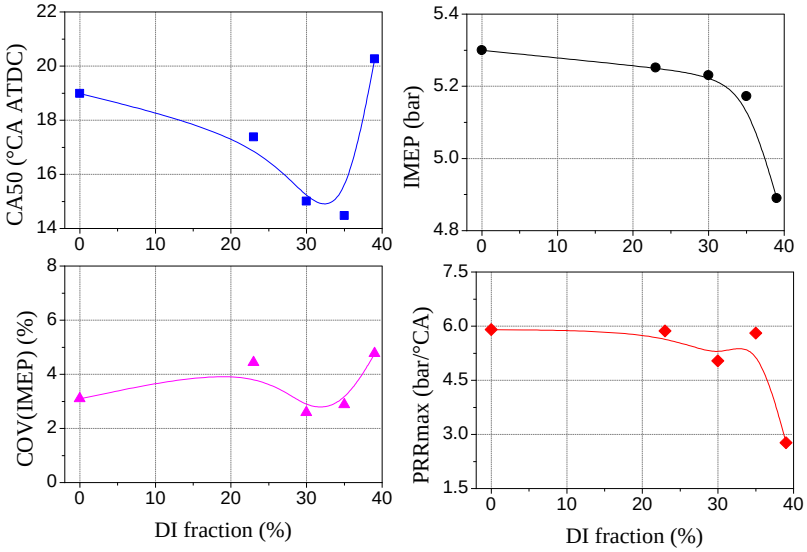

Fig. 6 Effect of DI fraction on CA50, IMEP, COV(IMEP), and PRR_{max}.

In addition, experiments with different DI fractions and STs were also performed. Fig. 7A shows a contour map for IMEP (gray background color) and CA50 (solid thin line). As shown, the knock limit (blue curve) and stability limit (red curve) can be identified by using the previously defined thresholds. Overall, as ST advanced, an earlier CA50 resulted in a higher IMEP at the risk of knocking combustion. On the other hand, an over-retarded ST could lead to an unstable combustion, as shown in Fig. 7. A lower DI fraction produced a higher IMEP at the same CA50, which could be attributed to the improved combustion process. However, the knocking combustion was significantly aggravated by the reduction in DI fraction, which finally led to the reduction in the admissible zone for the acceptable SFI hybrid combustion. This can be attributed to the strong auto-ignition

combustion of the in-cylinder mixture with less fuel stratification by using a small DI fraction. Therefore, in order to achieve the best fuel efficiency, a smaller DI fraction, such as 25% or 30%, is preferable as long as there is enough tolerance to knocking.

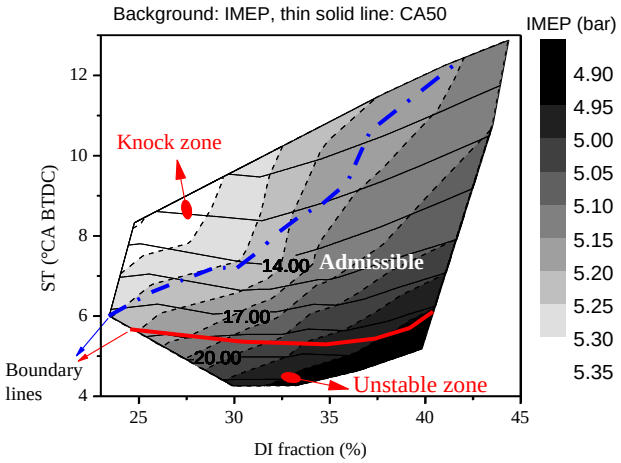

Fig. 7 Contour maps for IMEP and CA50 at different STs and DI fractions.

3.2.2 Effect of SOI timing

The sweep of the SOI timing was performed to determine its effect on the SFI hybrid combustion. Table 7 presents the operating conditions and Fig. 8 shows the corresponding HRR profiles at different SOI timings. As the SOI timing was delayed from 180 °CA BTDC to 140 °CA BTDC, the combustion phasing was almost kept constant with a slightly reduced peak HRR. As the SOI was delayed to 100 °CA BTDC, the combustion phasing was significantly delayed and the peak HRR was also reduced significantly, indicating a weaker early flame propagation and auto-ignition process. A further delay in SOI timing to 70 °CA BTDC slightly retarded the combustion phasing with a similar peak HRR. When the SOI timing was delayed to 50 °CA BTDC, the combustion phasing was significantly advanced with an increased peak HRR, indicating an enhanced SFI hybrid combustion process by a late DI.

Table 7. Operating conditions for the study on the effect of SOI timing.

Engine speed (rpm)	1500
Fuel rate (mg/stroke)	18.95
R_{DI} (%)	25
IVC (°CA ATDC)	584
EVC (°CA ATDC)	315
eEGR rate (%)	5
Intake manifold pressure (bar)	1.06–1.07
Spark timing (°CA BTDC)	7.5
Common rail pressure (bar)	80

Overall lambda	1

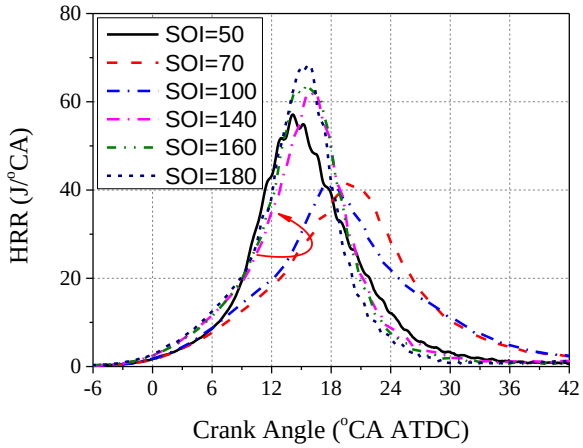

Fig. 8 Effect of SOI timing on HRR profile.

In order to determine the effects of SOI timing on the HRR profiles, the combustion process, duration of the early flame propagation stage (CA10–ST), duration of the main combustion stage (CA50–CA10), and duration of the late combustion stage (CA90–CA50) are shown in Fig. 9. From the figure, four zones can be identified:

1) In zone 1 (SOI ≤ 50 °CA BTDC), the durations of all stages were all shorter compared to those with SOI of 60 °CA BTDC. Although a late DI could result in an incomplete combustion due to the poor evaporation and air–fuel mixing process, the unburned fuel could turn into active species through the fuel reformation process during the NVO period and promote combustion in the next cycle [30]. Therefore, the SFI hybrid combustion was enhanced with the late SOI timing (SOI ≤ 50 °CA BTDC), leading to an advanced CA50 and higher PRR_{max} and IMEP values. In addition, the corresponding combustion process was also very stable with a COV(IMEP) value of approximately 2%.

2) In zone 2 (50 °CA BTDC ＜ SOI ≤ 90 °CA BTDC), CA50 was gradually retarded to approximately 19 °CA ATDC with an advance SOI timing. In addition, it was also found that the durations of all stages were gradually increased correspondingly in zone 2. This can be attributed to the weaker chemical effect of the active species from fuel reforming due to a better fuel–air mixing with the advance SOI timing. As a result, PRR_{max} was gradually reduced. Although COV(IMEP) was gradually increased with the advance SOI timing, it was still below the threshold (5%). It was also found that the IMEP value in zone 2 was slightly lower than that in zone 1, which can be attributed to the retarded CA50 in zone 2.

3) In zone 3 (90 °CA BTDC < SOI ≤ 140 °CA BTDC), the advance SOI timing led to an earlier CA50. The reason could be the suitable fuel stratification by advancing the SOI timing in zone 3, which enhanced the flame kernel growth and flame propagation and significantly reduced the duration of the early flame propagation stage (CA10–ST). In addition, the advance SOI timing could also reduce the fuel inhomogeneity and enhance the development of auto-ignition combustion. Therefore, the durations of the main combustion stage (CA50–CA10) and later combustion stage (CA90–CA50) were gradually reduced with the advance SOI timing. As a result, the advance CA50 resulted in a higher IMEP and better combustion stability at the expense of knocking, as shown in Fig. 9 (b).

4) In zone 4 (SOI > 140 °CA BTDC), the durations of all combustion stages were gradually increased with the advance SOI timing, resulting in a retarded CA50. The earlier SOI timing in zone 4 led to a more homogeneous fuel–air mixture due to a longer fuel–air mixing duration; this resulted in less enhancement of the early flame propagation. Therefore, the SFI hybrid combustion in zone 4 was similar to the PFI-enabled hybrid combustion, where the IMEP value was relatively higher with strong stability but at the risk of a high PRR_{max}, as shown in Fig. 9 (b).

Based on the above analysis, it was found that the SOI timings in zone 1 and zone 4 produced unacceptable PRR_{max} values and could not be used in real engine applications. In comparison, the SOI timings in zone 2 and zone 3 could be optimized to achieve a higher IMEP with acceptable PRR_{max} and COV(IMEP) values.

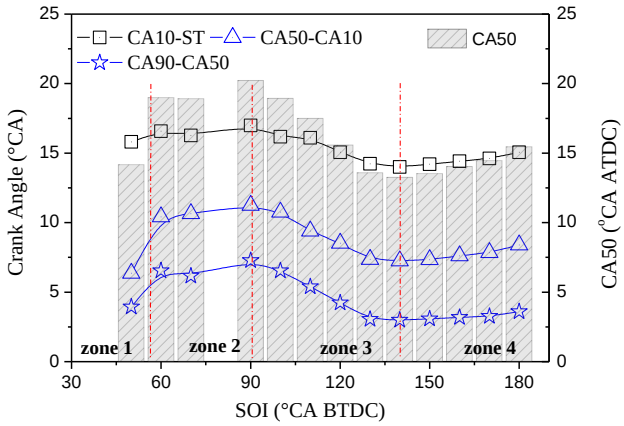

(a) Combustion phasing

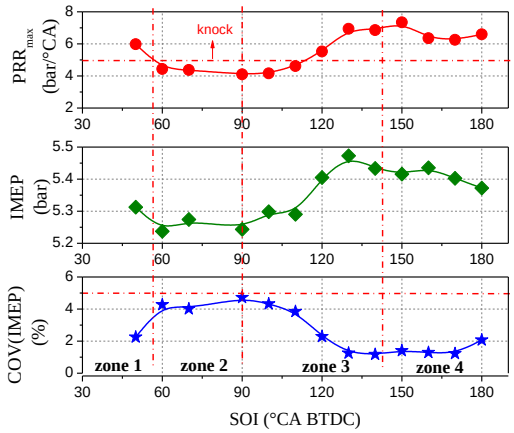

(b) PRR_{max}, IMEP, and COV(IMEP)

Fig. 9 Effects of SOI timing on (a) combustion phasing, (b) PRR_{max}, IMEP, and COV(IMEP).

Fig. 10 shows the contour map of IMEP and CA50 with different STs and SOI timings at a DI fraction of 25%. Detailed operating conditions are listed in Table 8. The background color represents the IMEP values, and the solid line indicates CA50. The knock limit with PRR_{max} = 5 bar/°CA and the stability limit with COV(IMEP) = 5% are also marked in the figure. As shown, a high-efficiency region with relatively higher IMEP values can be found in the right part of the admissible zone with relatively earlier STs and SOI timings. In real engine applications, the control strategy and corresponding algorithm should be appropriately designed to operate the engine within this admissible zone at a higher IMEP and acceptable PRR_{max} and combustion stability simultaneously.

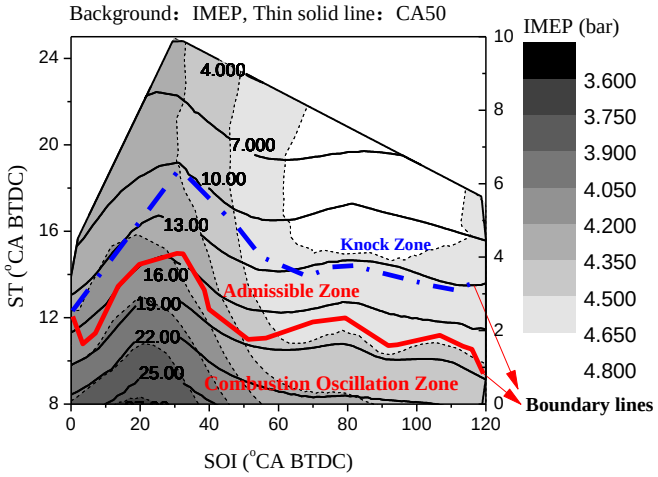

Fig. 10 Contour map of IMEP and CA50 at different STs and SOI timings.

Table 8. Operating conditions for the study on the effect of spark timing and SOI timing.

Engine speed (rpm)	1500
Fuel rate (mg/stroke)	17
DI fraction (%)	25
IVC (°CA ATDC)	584
EVC (°CA ATDC)	315
eEGR rate (%)	5
Intake manifold pressure (bar)	1.04–1.06
Rail pressure (bar)	80
Overall lambda (-)	1

4 Closed-loop control of SFI hybrid combustion

4.1 Development of the controller

The results discussed in Section 3 showed the potential of the SFI hybrid combustion to manage the EKS trade-off through adjustments in DI fraction and SOI timing. Compared to the DI fraction, the SOI timing showed much more complicated effects on the SFI hybrid combustion, as indicated by the different behaviors in the four zones in Fig. 9. In order to avoid the time-consuming offline calibration for the optimal SOI timings, an online optimization algorithm was developed by seeking the maximum value of a cost function (J) that mathematically represents the EKS trade-off.

$$J = J_\eta + \Gamma J_{PRR} = \frac{IMEP \times Vs}{LHV_f \times m_f} + \Gamma\left[\sigma_1 + \sigma_2 \exp(\sigma_3 \frac{PRR_{\max}}{PRR_{bound}} + \sigma_4)\right] \quad (1)$$

where m_f is the fuel rate (mg/stroke), $J_\eta = \frac{IMEP \times Vs}{LHV_f \times m_f}$ is the indicated thermal efficiency (η_i) of the engine, V_S is the engine displacement, σ_i (i = 1, 2, 3, and 4) are parameters for calibration, LHV_f is the lower heating value of gasoline, and $\Gamma = -1$. The exponential term, $J_{PRR} = \left[\sigma_1 + \sigma_2 \exp(\sigma_3 \frac{PRR_{\max}}{PRR_{bound}} + \sigma_4)\right]$, is a penalty term for PRR_{max}. A PRR_{bound} of 5 bar/°CA is used.

As shown in Fig. 11, the value of J_{PRR} is close to zero when PRR_{max} is less than 5 bar/°CA, indicating a little penalty of PRR_{max} on the output of the J function. At this condition, the optimization would be mainly focused on the thermal efficiency. However, if PRR_{max} exceeds 5 bar/°CA, the value of J_{PRR} would increase exponentially with PRR_{max}, leading to a smaller output of J as $\Gamma = -1$. Therefore, the optimization would have to be performed for both thermal efficiency and PRR_{max} in order to maximize the output of J. Fig. 12 shows the evolution of the value of J, thermal efficiency, and PRR_{max} with SOI timing. The

corresponding operating conditions are presented in Table 9. As shown in Fig. 12, the maximum value of the *J* function can be achieved with an SOI timing of 80 °CA BTDC. SOI timings earlier than 80 °CA BTDC resulted in lower values of *J* due to reduced thermal efficiency (η_i), while later SOI timings after that would also reduce the value of *J* due to the gradual increase in PRR_{max}.

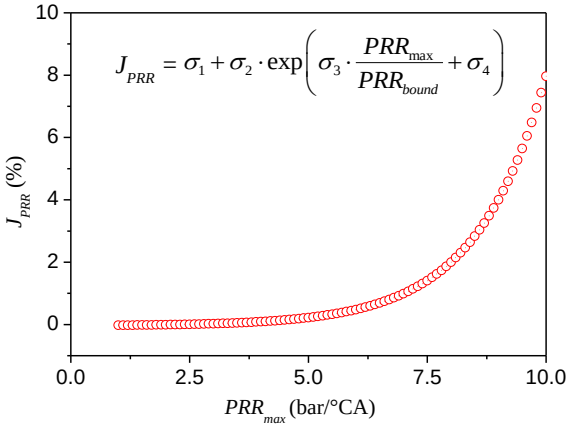

Fig. 11 Relation between PRR_{max} and $J_{PRR} = \sigma_1 + \sigma_2 \exp(\sigma_3 \frac{PRR_{max}}{PRR_{bound}} + \sigma_4)$, where σ_1 = 0.7, σ_2 = 0.29, σ_3 = 8.06e−4, σ_4 = −1.6e−3, and PRR_{bound} = 5 bar/°CA.

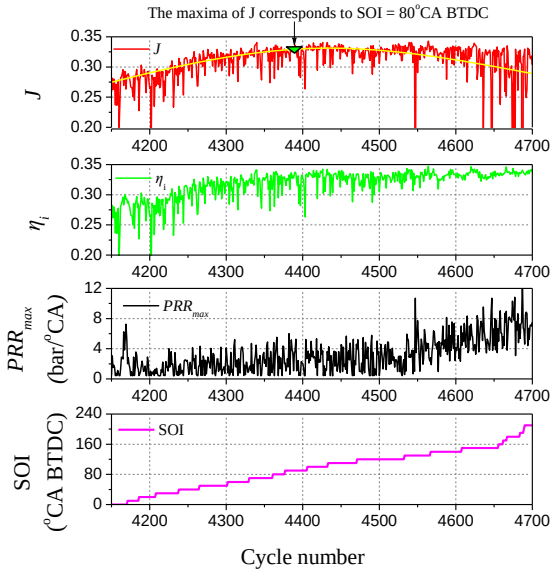

Fig. 12 Evolution of *J*, thermal efficiency (η_i), and PRR_{max} with SOI timing.

Table 9. Operating conditions for the study of the relationship between SOI timing and the J function.

Engine speed (rpm)	1500
Fuel rate (mg/cycle)	[17.5, 18]

DI fraction (%)	25
IVC (°CA ATDC)	585
EVC (°CA ATDC)	308
eEGR rate (%)	0
Intake manifold pressure (bar)	1.05–1.07
Common rail pressure (bar)	80
Spark timing (°CA BTDC)	[7.5, 17.5]
Overall lambda (-)	1

The above analysis also indicates that the optimization problem of the SOI timing and DI fraction can be directly converted into a maximum value-seeking problem for the *J* function. Therefore, a control structure for both SOI timing and DI fraction, as shown in Fig. 13, is proposed. The initial estimations of the DI fraction (R_{DI}) and SOI (SOI_{FF}) were obtained from lookup tables, namely MAP(R_{DI}) and MAP(SOI), respectively. The inputs of the maps were the engine speed (N_{Eng}) and total fuel rate (m_f); the outputs were the feedforward part of the DI fraction, i.e., R_{DI}, and the feedforward part of SOI, i.e., SOI_{FF}. MAP(R_{DI}) was calibrated to maximize the value of *J* with the SOI timing fixed at 100 °CA BTDC to simplify the calibration. Because a DI fraction of less than 23% was not achievable due to the limitation of the fuel flow rate control capability with the adopted solenoid injector, 23% was applied as the lower limit of R_{DI} in MAP(R_{DI}). Then MAP(R_{DI}) was used in the calibration of the SOI timing by maximizing the value of *J* and creating MAP(SOI_{FF}). To compensate for the inaccuracy in offline calibration of the SOI timing, an ES [29, 31] method was adopted by using the online optimization algorithm to adjust the SOI timing via the term SOI_{FB} based on the *J* function. By using the cylinder pressure (*p*), IMEP and PRR_{max} were obtained through the combustion analysis module and were then used as inputs to the *J* function. The gradient of the *J* function with respect to SOI, i.e., $\frac{\partial J}{\partial (SOI)}$, was obtained via a combination of a high pass filter ($\frac{\tau_{HP} s}{\tau_{HP} s + 1}$) and a low pass filter ($\frac{\tau_{LP}}{\tau_{LP} s + 1}$). Here, τ_{HP} and τ_{LP} are the time constants of the high pass and low pass filters, respectively. The term $\frac{\partial J}{\partial (SOI)}$ was then fed into the optimizer, i.e., $\frac{\varepsilon / a_{ES}}{s}$, to yield the correction term SOI_0, where ε is the gain to be tuned. SOI_0, in combination with the sinusoidal dither signal $\Delta SOI_{FB} = a_{ES} \cdot \sin(\omega t)$, created the feedback part of SOI, i.e., SOI_{FB}, where a_{ES} is the magnitude of the sinusoidal signal to be

tuned. The variation of SOI_{FB} then forced the SOI to converge to the optimal value that maximized the J function in the negative gradient direction following SOI = SOI_{FF} + SOI_{FB}.

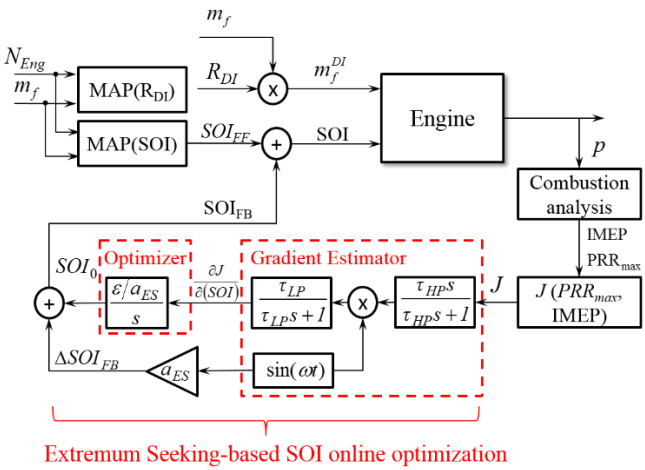

Fig. 13 Proposed control structure for DI fraction and SOI timing.

4.2 Experimental validation

To achieve a real-time control, the parameters of the proposed controller have to be tuned. The tuning method is described as follows and the controller parameters used are as listed in Table 10.

1) The convergence speed of the ES algorithm can be improved by increasing ε , a_{ES}, τ_{HP}, or τ_{LP}. However, this could also lead to increased oscillation of the SOI timing.

2) There is a constraint on the frequency of the sinusoidal exiting signal $\alpha_{ES}sin(\omega t)$: $2\pi\omega$ should be within the pass band of the low pass filter and the high pass filter, i.e., $\tau_{LP} < 2\pi\omega < \tau_{HP}$.

3) There is a constraint on the amplitude of the sinusoidal signal: a_{ES} should be much smaller than the SOI timing, i.e., a_{ES} < SOI.

4) σ_i (i =1, 2, 3, and 4) and Γ should be tuned to achieve an appropriate trade-off between PRR_{max} and thermal efficiency, as shown in Fig. 11 and Fig. 12.

Table 10. Controller parameters.

τ_{LP} (s)	ω (rad/s)	a_{ES}	τ_{HP} (s)	ε	σ_1	σ_2	σ_3	σ_4	Γ
2	6.28	3	8	3000	0.7	0.29	8.06e−4	−1.60e−3	−1

The proposed controller was then validated in experiments with the tuned controller parameters. The operating conditions are given in Table 11. The controller was implemented in Matlab/Simulink and operated in the MicroAutobox, a prototype

controller with a process frequency of 800 MHz, as shown in Fig. 2. The computational time of the controller is less than 0.1 ms with the random-access memory and read-only memory less than 500 bytes and 1.3 kB respectively, showing a great potential for real-time applications.

Two operating conditions with STs of 5 °CA BTDC and 7 °CA BTDC were used to validate the performance of the proposed controller. As shown in Fig. 14, the SOI timing converged to 82 °CA BTDC with an ST of 5 °CA BTDC and 52 °CA BTDC with an ST of 7 °CA BTDC, based on the same SOI_{FF} of 25 °CA BTDC. In the optimization process, the values of J and hence IMEP increased gradually and then became steady afterward. It was also noted that the value of J for an ST of 7 °CA BTDC was lower than that with an ST of 5 °CA BTDC, which could be attributed to the higher PRR_{max} due to an earlier combustion phasing. In addition, the high PRR_{max} with an ST of 7 °CA BTDC also led to a higher oscillation of J due to the effect of the $\left[\sigma_1+\sigma_2\exp(\sigma_3\frac{PRR_{\max}}{PRR_{bound}}+\sigma_4)\right]$ term. Note that the ST in the test was randomly chosen from an admissible range, where a stable combustion can be maintained at SOIs ranging from 180 °CA BTDC to 0 °CA BTDC. It was found that the proposed controller automatically drove the SOI from zone 1 (SOI ≤ 50 °CA BTDC) to zone 2 via online optimization, achieving higher IMEP with acceptable PRR_{max}. This was in line with the intention as discussed in Section 3.2.2, i.e., to control the SOI in zones 2 and 3 (50 °CA BTDC ≤ 1SOI ≤ 140 °CA BTDC) for better ESK trade-off.

Table 11. Operating conditions for the experimental validation.

	Case 1	Case 2
Engine speed (rpm)	1500	1500
DI fraction (%)	30	30
IVC (°CA ATDC)	589	589
EVC (°CA ATDC)	310	310
eEGR valve opening (%)	15	15
Intake manifold pressure (bar)	1.06	1.06
Common rail pressure (bar)	80	80
Spark timing (°CA BTDC)	5	7
Overall lambda (-)	1	1

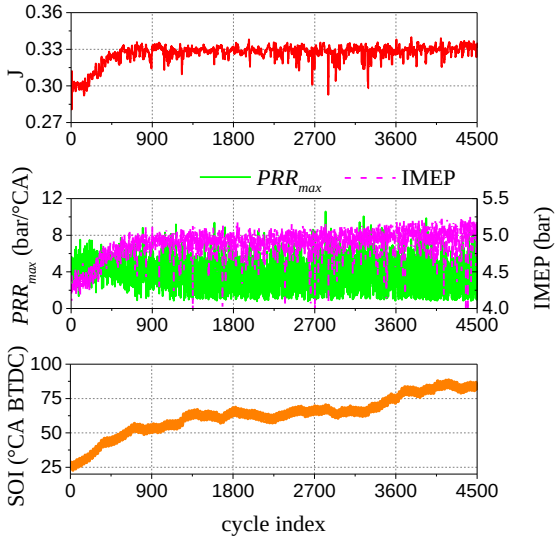

a) Spark timing at 5 °CA BTDC.

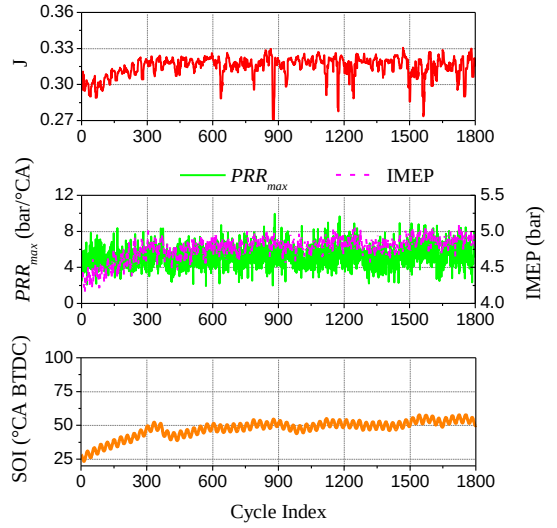

b) Spark timing at 7 °CA BTDC

Fig. 14 Control performance of the online optimization algorithm.

5 Conclusions

In this study, SFI hybrid combustion was realized in a four-cylinder gasoline engine equipped with the P-DI system. The P-DI strategy was compared to the pure PFI and DI strategies with the SI-CAI hybrid combustion. The effects of the DI fraction and SOI timing on the fuel EKS trade-off were analyzed in detail. To manage the EKS trade-off in real-time, an online optimization algorithm was developed and used to validate the SOI timing. The main conclusions are summarized as follows.

1) Compared to the SI-CAI hybrid combustion with pure PFI and DI strategies, the P-DI-enabled SFI hybrid combustion showed an improved fuel economy. In the operating window defined by the knock and combustion instability limits, the average fuel economy of the P-DI strategy showed 0.4% and 2.5% improvements compared to the pure PFI and DI strategies, respectively. The analysis of HRR profiles indicated that the P-DI strategy could be used to promote the flame kernel and flame propagation, while moderating the subsequent auto-ignition combustion with lower PRR_{max}.

2) For a fixed SOI timing, increasing the DI fraction advanced the SFI hybrid combustion process when the DI fraction was less than 35%. This can be attributed to the enhanced early SI combustion. A further increase in the DI fraction to 39% significantly delayed the SFI hybrid combustion phasing.

3) Four zones were defined to investigate the effect of SOI timing on the SFI hybrid combustion process. An earlier SOI timing led to an earlier combustion phasing in zone 1 (SOI ≤ 50 °CA BTDC), while an earlier SOI timing in zone 4 (SOI > 140 °CA BTDC) resulted in a delayed combustion phasing. In zone 3 (90 °CA BTDC < SOI ≤ 140 °CA BTDC), an earlier SOI advanced the combustion phasing. Zone 2 was between zones 1 and 3, and it was found that the SFI hybrid combustion achieved the most delayed combustion phasing and lowest PRR_{max} in this zone.

4) To control the P-DI-enabled SFI combustion, the EKS trade-off relationship was represented by a cost function (J) based on the findings of the effects of SOI timing on the combustion process. By seeking the maximum value of the cost function with the ES algorithm, an online optimization algorithm was developed for the optimal SOI timing. Experimental validation showed that the SOI timing was able to converge to the optimal value under different STs, verifying the applicability of the proposed control algorithm for P-DI-enabled SFI hybrid combustion.

Acknowledgments

This work was supported by the National Natural Science Foundation of China (Grant number: 51376135) and the State Key Project of Fundamental Research Plan (Grant number 2013CB228403).

The authors would also like to thank Prof. Hua Zhao at Brunel University London for the suggestions on this work and Dr. Tao Chen and Kang Xu at State Key Laboratory of Engines in Tianjin University for the useful discussions.

Nomenclature

ATDC	After top dead center

BTDC	Before top dead center
CA	Crank angle
CA10	Crank angle at 10% total heat release
CA50	Crank angle at 50% total heat release
CAI	Controlled auto-ignition
COV	Coefficient of variation
DI	Direct injection
EGR	Exhaust gas recirculation
eEGR	External exhaust gas recirculation
EKG	Early kernel growth
EKS	Fuel economy-knock-combustion stability
EVC	Exhaust valve closing
ES	Extremum seeking
MFB	Mass fraction burnt
HRR	Heat release rate
IMEP	Indicated mean effective pressure
IVC	Intake valve closing
J	The proposed cost function for injection timing optimization
NVO	Negative valve overlap
P-DI	Port-direct injection
PFI	Port fuel injection
PRR	Pressure rise rate
R_{DI}	The fraction of fuel mass from DI in the total fuel mass
SFI	Stratified flame ignition
SI	Spark-ignition
ST	Spark timing
SOI	Start of injection (for direct injection)
Vs	Engine displacement volume
η_i	Indicated thermal efficiency
τ	Time constant
σ_i	Parameters for calibration in the proposed cost function
Subscript	
DI	Direct injection
ES	Extremum seeking
FF	Feedforward control
FB	Feedback control
HP	High pressure
LP	Low pressure

max	The maximum value

References

1. Zhao H. HCCI and CAI engines for the automotive industry. Cambridge (England): Woodhead Publishing; 2007.

2. Maurya, Rakesh Kumar, and Avinash Kumar Agarwal. Experimental investigation on the effect of intake air temperature and air – fuel ratio on cycle-to-cycle variations of HCCI combustion and performance parameters. *Appl Energy* 2011;88 (4): 1153-1163.

3. Yang D, Wang Z, Wang J, Shuai S. Experimental study of fuel stratification for HCCI high load extension. *Appl Energy* 2011;88(9):2949 – 54.

4. Li N, Xie H, Chen T, et al. The effects of intake backflow on in-cylinder situation and auto ignition in a gasoline controlled auto ignition engine. *Appl Energy* 2013; 101(1):756-764.

5. Chen T, Xie H, Li L, et al. Methods to achieve HCCI/CAI combustion at idle operation in a 4VVAS gasoline engine. *Appl Energy*, 2014, 116(3):41-51.

6. Xie H, Yang L, Qin J, et al, The effect of spark ignition on the CAI combustion operation, SAE technical paper 2005-01-3738; 2005.

7. Wang Z. Wang Z, He X, Wang J, Shuai S, Xu F, Yang D. Combustion visualization and experimental study on spark induced compression ignition (SICI) in gasoline HCCI engines. *Energy Convers Manage* 2010; 51: 908 – 917.

8. Olesky L M, Lavoie G A, Assanis D N, Wooldridge M S, Martz J B. The effects of diluent composition on the rates of HCCI and spark assisted compression ignition combustion. *Appl Energy* 2014; 124(0): 186 - 198.

9. Chen T, Xie H, Le Li, Yu W, Li Z, Zhao H. Continuous load adjustment strategy of a gasoline HCCI-SI engine fully controlled by exhaust gas. SAE technical paper 2011-01-1408; 2011.

10. Zhang, Y, Xie, H, Zhou, N, Chen, T, Zhao, H. Study of SI-HCCI-SI transition on a port fuel injection engine equipped with 4VVAS. SAE Technical Paper 2007-01-0199; 2007.

11. Manofsky L, Vavra J, Assanis D, Babajimopoulos A. Bridging the gap between HCCI and SI: spark-assisted compression ignition. SAE technical paper 2011-01-1179; 2011.

12. Middleton RJ, Olesky LK. et al., The effect of spark timing and negative valve overlap on Spark Assisted Compression Ignition combustion heat release rate. *Proc Combust Inst* 2015; 35(3): 3117-3124.

13. Olesky L M, Martz J B, Lavoie G A, Vavra J, Assanis D N, Babajimopoulos A. The effects of spark timing, unburned gas

temperature, and negative valve overlap on the rates of stoichiometric spark assisted compression ignition combustion. *Appl Energy* 2013; 105(0): 407-417.

14. Wang X, Xie H, Li L, Xie L, Chen T, Zhao H. Effect of the thermal stratification on SI – CAI hybrid combustion in a gasoline engine. *Appl Therm Eng* 2013;61 (2):451 – 60.

15. Xie H, Le Li, Chen T, Yu W, Wang X, Zhao H. Study on spark assisted compression ignition (SACI) combustion with positive valve overlap at medium – high load. *Appl Energy* 2013;101:622 – 33.

16. Yun H, Wermuth N, Najt P, Extending the high load operating limit of a naturally-aspirated gasoline HCCI combustion engine. SAE technical paper 2010-01-0847; 2010.

17. Yoshizawa K, Teraji A, Miyakubo H, Yamaguchi K, Urushihara T. Study of high load operation limit expansion for gasoline compression ignition engines. *J Eng Gas Turbines Power* 2006;128(2):377 – 87.

18. Reuss D L, Kuo T W, Silvas G, et al. Experimental metrics for identifying origins of combustion variability during spark-assisted compression ignition. *Int J Engine Res* 2008, 9(5): 409-434.

19. Natarajan VK, Sick V, Reuss DL, et al. Effect of spark-ignition on combustion periods during spark-assisted compression ignition. *Combust Sci Technol* 2009; 181(9): 1187-1206.

20. Wang X, Xie H, Zhao H. Computational Study of the Influence of In-cylinder Flow on SI-CAI Hybrid Combustion in a Gasoline Engine. *Int J Engine Res.* 2014; 16(6): 795-809.

21. Chen T, Zhao H, Xie H. Analysis of cyclic variations during mode switching between spark ignition and controlled auto-ignition combustion operations. *Int J Engine Res.* 2014; (16): 255-259.

22. Hellstrom E, Stefanopoulou A, Vavra J, et al. Understanding the dynamic evolution of cyclic variability at the operating limits of HCCI engines with negative valve overlap. *SAE Int J Engines* 2012; 5: 995-1008.

23. Ma S, Zheng Z, Liu H, Zhang Q, Yao M. Experimental investigation of the effects of diesel injection strategy on gasoline/diesel dual-fuel combustion. *Appl Energy* 2013;109:202 – 12.

24. Jang J, Lee J, Kim J, et al. Comparisons of the nanoparticle emission characteristics between GDI and PFI vehicles. *Journal of Nanoparticle Research* 2015, 17(12):1-14.

25. Wang X, Zhao H, Xie H. Effect of piston shapes and fuel injection strategies on stoichiometric stratified flame ignition (SFI) hybrid combustion in a PFI/DI gasoline engine by numerical simulations. *Energy Convers Manage* 2015;98:387 – 400.

26. Wang X, Zhao H, Xie H. Effect of dilution strategies and direct injection ratios on stratified flame ignition (SFI)hybrid

combustion in a PFI/DI gasoline engine *Appl Energy*, 2016, 165:801-814.

27. Knop V, Essayem E. Comparison of PFI and DI Operation in a Downsized Gasoline Engine. *SAE Int J Engines* 2013, 6(6):941-952.

28. Persson H. Study of Fuel Stratification on Spark Assisted Compression Ignition (SACI) Combustion with Ethanol Using High Speed Fuel PLIF. SAE Technical Paper 2008-01-2401; 2008.

29. Tan Y, Moase W H, Manzie C. Extremum Seeking From 1922 To 2010. Chinese Control Conference (CCC), Beijing, China; 29-31 July 2010. 14-26.

30. Yu W, Xie H, Chen T. Effects of Active Species in Residual Gas on Auto- Ignition in a HCCI Gasoline Engine. SAE Techincal Paper 2012-01-1115.

31. Bodrov V A, Zarakovskiĭ G M. Engineering psychological principles of optimizing the control systems of flying vehicles. Kosmicheskaia Biologiia I Aviakosmicheskaia Meditsina, 1978, 12(2):8.